Molecular Transport into Mesostructured Silica Thin Films: Electrochemical Monitoring and Comparison between *p*6*m*, P6$_3$/*mmc*, and *Pm*3*n* Structures

Mathieu Etienne,[†] Alida Quach,[‡] David Grosso,[‡] Lionel Nicole,[‡] Clément Sanchez,*[,‡] and Alain Walcarius*[,†]

Laboratoire de Chimie Physique et Microbiologie pour l'Environnement, Unité Mixte de Recherche UMR 7564, CNRS−Nancy-Université, 405 rue de Vandoeuvre, F-54600 Villers-lès-Nancy, France, and Laboratoire de Chimie de la Matière Condensée, Unité Mixte de Recherche UMR 7574, CNRS−Université Pierre et Marie Curie, 4 place Jussieu, 75 252 Paris Cedex 05

Received October 20, 2006. Revised Manuscript Received December 12, 2006

Ellipso-porosimetry and electrochemical techniques were used to characterize porosity and molecular transport into mesostructured porous silica thin films displaying various structures. The films have been prepared by the evaporation-induced self-assembly (EISA) method using cetyltrimethylammonium bromide (CTAB) as the template. According to previous investigations, the structure of the film can be controlled by the fine adjustment of the CTAB concentration and relative humidity during the dip-coating process. Films displaying *p*6*m* (2D hexagonal), *P*6$_3$/*mmc* (3D hexagonal), and *Pm*3*n* (cubic) nanoporous structures have been obtained (as revealed by XRD and TEM) and characterized after template removal by ethanol washing. Characterization of the film porosity has been performed on the basis of water adsorption−desorption cycles and ellipso-porosimetry measurements. They revealed significant contraction of the mesoporous structure when contacting water molecules, leading to a decrease in the pore diameter for both 3D hexagonal and cubic mesostructures and to an important damaging of the 2D hexagonal mesostructure. Another mesoporous silica film prepared with a block copolymer (F127), displaying a cubic structure (*Im*3*m*), was used for comparison purposes. Electrochemical investigations by cyclic voltammetry and wall-jet electrochemistry were performed using electrochemical probes displaying various charges and sizes (I^-, $Fe(CN)_6^{3-}$, $Ru(bpy)_3^{2+}$, FcMeOH). The organization of the porous network constituting the silica film and its stability in aqueous medium were found to have a profound effect on its permeability properties, and the following sequence was observed by cyclic voltammetry: *Pm*3*n* > *P*6$_3$/*mmc* ≈ *Im*3*m* > *P*6*m*. The electrochemical responses were also dramatically influenced by the charge and to a lesser extent the size of the molecular probe. Positively charged species ($Ru(bpy)_3^{3+/2+}$ and oxidized FcMeOH) were likely to accumulate in the film, whereas negatively charged species ($Fe(CN)_6^{3-}$, I^-) could be totally or partially excluded, leading to either preconcentration or permselective behaviors. Quantitative evaluation of the permeability (PD_f, where P is the partition coefficient and D_f the apparent diffusion coefficient in the film) of the different molecular probes in thin films displaying a cubic mesostructure was achieved using the wall-jet electrochemistry technique. The obtained values (in the 1×10^{-8} to 1×10^{-7} cm^2 s^{-1} range) were discussed with respect to the probe size and charge. The results presented in this article can be useful in the various fields that promote the use of mesoporous silica layers for sensing, membranes, chromatography, catalysis, and electrochemical-cell-based applications.

1. Introduction

The preparation of silica-based mesoporous thin films via the sol−gel process has been the subject of intense research during the past decade. Ogawa[1] was the first to have described the preparation of a mesoporous silica thin film by spin-coating it on a solid substrate. In this case, the mesoporous channels were arranged parallel to the substrate with a hexagonal symmetry comparable to that observed in MCM-41 material, which was discovered by the Mobil Oil Company and described 2 years before.[2] However, this 2D arrangement was not optimal for most applications requiring effective mass-transfer processes through the mesoporous thin film, and much effort has been made to prepare thin films with 3D organization.

Some years after, Lu et al.[3] succeeded in preparing continuous supported cubic mesoporous silica thin films by sol−gel dip-coating. Fine-tuning of the conditions for film formation (especially the surfactant concentration) yielded high-quality, pinhole-free films with desired thicknesses. Mesostructuration of the material occurred during the so-called evaporation-induced self-assembly (EISA) of the silica

* Corresponding author. Fax: 33 3 83 27 54 44 (A.W.); 33 1 44 27 47 69 (C.S.). E-mail: Walcarius@lcpme.cnrs-nancy.fr (A.W.); clems@ccr.jussieu.fr (C.S.).

[†] CNRS−Université H. Poincaré Nancy I.

[‡] CNRS−Université Pierre et Marie Curie.

(1) Ogawa, M. *J. Am. Chem. Soc.* **1994**, *116*, 7941.

(2) Kresge, C. T.; Leonowicz, M. E.; Roth, W. J.; Vartuli, J. C.; Beck, J. S. *Nature* **1992**, *359*, 710.

(3) Lu, Y.; Ganguli, R.; Drewien, C. A.; Anderson, M. T.; Brinker, C. J.; Gong, W.; Guo, Y.; Soyez, H.; Dunn, B.; Huang, M. H.; Zink, J. I. *Nature* **1997**, *389*, 364.

10.1021/cm0625068 CCC: $37.00
Published on Web 01/26/2007

monomers.[4] Following a similar procedure, Sanchez and coworkers were able to clearly identify the different parameters influencing the final structure of the mesoporous films prepared by the EISA process.[5] It appears that during the dip-coating step, the relative humidity into the chamber for film deposition has a strong influence on the final structure of the film.[6] According to all these studies, it is now possible to prepare mesoporous thin films with 2D hexagonal (*p*6*m*), 3D hexagonal ($P6_3/mmc$), and cubic (*Pm*3*n*) structures, using cetyltrimethylammonium bromide (CTAB) as structuring agent and operating under controlled humidity conditions.[5−7]

In parallel, silica-based materials have found several exciting applications in the field of electrochemistry (and the ordered mesoporous ones hold a prominent position).[8] The main reasons for such a craze for the implication of mesoporous (organo)silica in electrochemical science are related to the attractive characteristics of these mesostructured solids, especially the high and fast accessibility to numerous active centers located in regular mesopore channels and the host properties of these materials for a wide range of guest (bio)molecules (redox probes, complexing ligands, enzymes, ...).[9] Actually, most of these investigations were based on bulk composite electrodes (mesoporous particles dispersed into a conductive composite matrix) as well as on film-type electrodes (mesoporous materials deposited onto the surface of a solid electrode). Two categories have to be distinguished in this latter case: (1) powdered mesoporous silica deposits (together with a polymer binder or overcoating to ensure mechanical stability) and (2) continuous mesoporous silica films directly prepared on the electrode surface. This last category appears as the most promising (because it is binder-free), but electrochemical measurements at thin film modified electrodes can be performed efficiently only if the film does not prevent access to the electrode surface (i.e., enabling effective mass transport through the film, from the solution toward the electrode surface, and/or electron transfer at the electrode−film interface). From this point of view, it is thus of major importance to control the mesoporous structure of films on electrode surfaces.

Electrochemistry with mesoporous silica thin films is still in its infancy. Song and Villemure[10] have reported a pioneering electrochemical investigation of such films prepared on indium-tin-oxide (ITO) electrodes by adapting a procedure from Ogawa.[1] As the films were characterized by a 2D hexagonal mesostructure with a one-dimensional channel orientated parallel to the ITO substrate, they completely prevented the electrochemical detection of the negatively charged redox probe $Fe(CN)_6^{3-}$ while exhibiting a slow accumulation of the positively charged $Ru(bpy)_3^{2+}$ species, as otherwise reported for clay modified electrodes.[11] Some other works have involved mesoporous thin films on electrode surfaces for heavy metal detection[12] or photoregulation of mass transport by use of mesoporous silica modified by a photoresponsive molecule.[13] We have recently provided an electrochemical study of organically modified mesoporous silica thin films deposited on various electrodes substrates (gold, platinum, and glassy carbon)[14] as well as a report on the use of electrochemistry to evidence morphological transformations in ordered mesoporous titanium oxide thin films.[15] To date, however, no investigation on the effect of the mesoporous structure on the response of the modified electrodes has been provided, in spite of its expected great influence on the electrochemical device sensitivity.

In the present work, we have thus prepared several mesoporous silica thin films with various well-defined structures (2D hexagonal, 3D hexagonal, cubic) and several thicknesses and displayed them on ITO electrodes. They were carefully characterized with XRD, TEM, ellipsometry, cyclic voltammetry, and wall-jet hydrodynamic electrochemistry. The electrochemical responses were analyzed in terms of permeation to various redox probes[16] in order to discuss how the different structures would affect mass-transfer processes into these films. Redox probes were selected on the basis of their different charges and sizes (I^-, $Fe(CN)_6^{3-}$, ferrocene methanol, and $Ru(bpy)_3^{2+}$ with bpy = bipyridine).

2. Experimental Section

2.1. Chemical and Reagents. Potassium hexacyanoferrate(III) ($K_3Fe(CN)_6$, Fluka), potassium iodide (KI, Prolabo), ferrocene methanol, (FcMeOH, Aldrich), and potassium hydrogen phthalate (KHP, Merck) were analytical grade. Tris(2,2′-bipyridine)ruthenium(II) chloride hexahydrate ($Ru(bpy)_3Cl_2 \cdot 6H_2O$) was purchased from Acros Organic and used as received. All solutions were prepared with high-purity water (18 MΩ cm^{-1}) from a Millipore milli-Q water purification system. Tetraethoxysilane (TEOS), cetyltrimethylammonium bromide (CTAB), and tetraoctylammonium bromide (TOAB) were used for film preparation.

2.2. Film Electrode Preparation. Mesoporous silica thin films were prepared with CTAB as the structuring agent. As reported elsewhere,[7] silicon ethoxide, ethanol, acidic water, and surfactant were mixed together, leading to a final molar composition of 1:20:0.004:5:0.10−0.18 TEOS:EtOH:HCl:H_2O:CTAB. In some cases, CTAB was partially replaced by tetraoctylammonium bromide so as to obtain ratios of 1:0.12:0.1 TEOS:CTAB:TOAB. Sols were aged at room temperature for 4 days prior to deposition on single-side-polished, 525 μm thick silicon wafers and ITO slides (Delta Technologies, Stillwater, MN; surface resistivity = 4−8 Ω),

(4) Brinker, J. B.; Lu, Y.; Sellinger, A.; Fan, H. *Adv. Mater.* **1999**, *11*, 579.
(5) Grosso, D.; Babonneau, F.; Albouy, P. A.; Amenitsch, H.; Balkenende, A. R.; Brunet-Bruneau, A.; Rivory, J. *Chem. Mater.* **2002**, *2*, 931.
(6) Cagnol, F.; Grosso, D.; Soler-Illia, G. J. de A. A.; Crepaldi, E. L.; Babonneau, F.; Amenitsch, H.; Sanchez, C. *J. Mater. Chem.* **2003**, *13*, 61.
(7) Grosso, D.; Cagnol, F.; Soler-Illia, G. J. A. A.; Crepaldi, E. L.; Amenitsch, H.; Brunet-Bruneau, A.; Bourgeois, A.; Sanchez, C. *Adv. Funct. Mater.* **2004**, *14*, 309.
(8) (a) Walcarius, A. *C. R. Chim.* **2005**, *8*, 693. (b) Walcarius, A.; Mandler, D.; Cox, J.; Collinson, M. M.; Lev, O. *J. Mater. Chem.* **2005**, *15*, 3716.
(9) Walcarius, A.; Etienne, M. In *Handbook of Electrochemical Nanotechnology*; Lin, Y., Nalwa, H. S., Eds.; American Scientific Publishers: Stevenson Ranch, CA, 2007.
(10) Song, C.; Villemure, G. *Microporous Mesoporous Mater.* **2001**, *44−45*, 679.
(11) Fitch, A. *Clays Clay Miner.* **1990**, *38*, 391−400.
(12) Yantasee W.; Lin Y.; Li X.; Fryxell G. E.; Zemanian T. S.; Viswanathan V. V. *Analyst* **2003**, *128*, 899.
(13) Liu, N.; Dunphy, D. R.; Atanassov, P.; Bunge, S. D.; Chen, Z.; Lopez, G. P.; Boyle, T. J.; Brinker, C. J. *Nano Lett.* **2004**, *4*, 551.
(14) Etienne, M.; Walcarius, A. *Electrochem. Commun.* **2005**, *7*, 1449.
(15) Etienne, M.; Grosso, D.; Boissière, C.; Sanchez, C.; Walcarius, A. *Chem. Commun.* **2005**, 4566.
(16) Bard, A. J.; Faulkner, L. R. *Electrochemical Methods: Fundamentals and Applications*, 2nd ed.; John Wiley and Sons: New York, 2000.

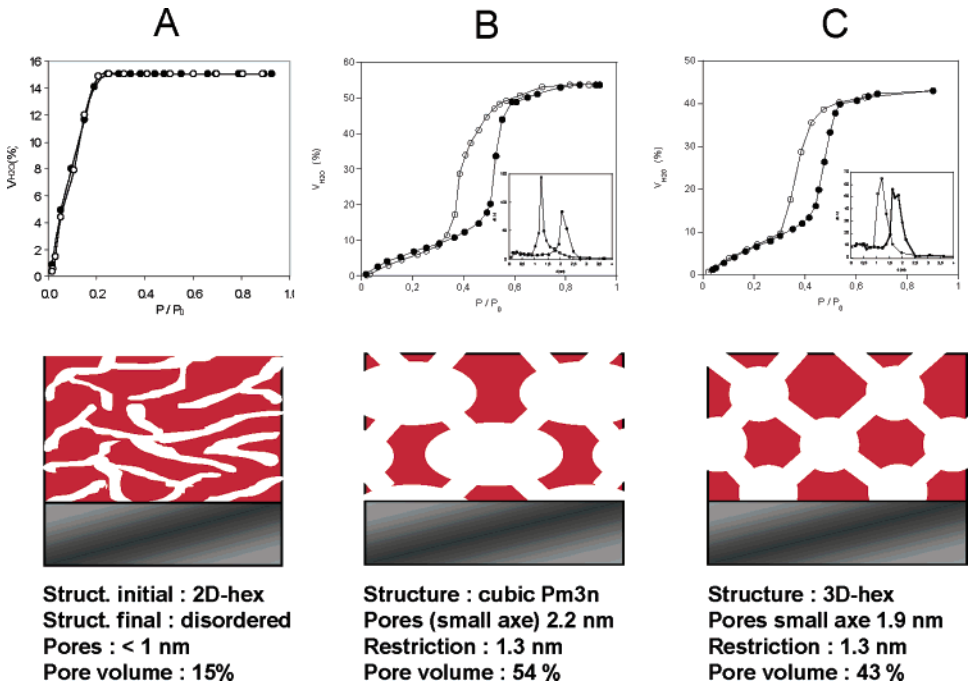

Figure 1. Water adsorption−desorption, pore size distribution (PSD), model of structure and porosity characteristics of the three systems used for electrochemical analyses: (A) "2D-Hex-Col", (B) cubic, and (C) 3D hexagonal.

subsequently used for ellipsometric and electrochemical characterizations. The substrates were dip-coated at different withdrawal rates (1.7, 2.7, and 3.7 mm s^{-1}), with higher speeds yielding thicker films. To obtain the highest level of ordering and optical quality, the relative humidity (RH) inside the deposition chamber was carefully controlled between 40 and 70%, depending on the desired mesophase.[7] The films were stabilized at 130 °C for at least 2 days and then rinsed with ethanol (simple nozzle with the aid of a washing bottle) to remove surfactant. An additional sample with larger pores was prepared as previously described[17] by using a F127 Pluronic block copolymer template, which was extracted by calcination prior to use.

2.3. Instrumentation and Analytical Procedures. Mesostructures were deduced from Bragg−Brentano X-ray diffractograms recorded with a Philips PW 1830 device. Porosity measurements were carried out on a Woolam UV−visible variable angle spectroscopic ellipsometer (WVASE) coupled with a WVASE32 data analysis software. The setup included an environment control cell into which a continuous flux of air at a fixed partial pressure of water was insufflated. The evolutions of the layer's refractive index and thickness were monitored and the adsorbed water volume was calculated using the Bruggemann effective medium approximation.[17] The experimental protocol (determination of pore anisotropy, creation of a water adsorption−desorption isotherm, calculation of porous parameters and Young modulus) as well as the pore contraction model are dealt with in detail in a separate article.[17]

All electrochemical measurements have been performed with a PGSTAT12 Autolab potentiostat monitored by GPES electrochemical software (general purpose electrochemical system, Eco Chemie) in a conventional three-electrode cell. The working electrode was the ITO-modified electrode, usually used after template removal from the mesoporous film by ethanol washing. The surface of the electrode was delimited by a O-ring (1 mm thick and 9 mm inner diameter, or 0.5 mm thick and 8 mm inner diameter) on which was placed a Teflon reservoir containing the electrolyte solution. A Pt wire served as the counter electrode and an Ag/AgCl electrode (Metrohm) was used as the reference. Mass transport of electroactive species into mesoporous silica thin films has been studied using cyclic voltammetry at various scan rates, ranging from 5 to 250 mV s^{-1}. Most reported figures correspond to experiments performed at 50 or 100 mV s^{-1}. Solutions were made of $Fe(CN)_6^{3-}$, $Ru(bpy)_3^{2+}$, FcMeOH, and I^- in KHP buffer (0.05 M, pH 4.1).

Some experiments directed to quantitative analysis of permeability into the cubic phase mesoporous thin films have been carried out using a home-built wall-jet electrochemical setup. It consisted of a syringe needle positioned 1 mm from the analyzed electrode, perpendicular and pointing out of the center of the electrode surface area defined by a O-ring (0.5 mm thick and 8 mm inner diameter). A Pt wire served as a counter electrode and an Ag wire coated with AgCl was used as a pseudo-reference electrode. Volume flow rates (V) were controlled by a peristaltic pump. Note that this particular electrochemical cell was also used for performing several cyclic voltammetry experiments, especially those requiring equilibration with the external solution prior to measurement, which was achieved by flowing the solution for some minutes on the electrode surface.

3. Results and Discussion

3.1. Structure and Porosity Characterization. In the first part of this study, the porous structure and related mechanical stability of CTAB templated films, bearing 3D hexagonal $P6_3/mmc$, cubic $Pm3n$, or 2D hexagonal $P6m$ are assessed using environmental ellipsometry analysis. Structural information concerning the specific arrangement of the nanopores within the inorganic network has been completely analyzed by XRD and TEM (see Figures A−D in the Supporting Information), and the results are consistent with those reported in previous papers.[7] In the present work, after surfactant leaching, films were allowed to equilibrate within increasing relative humidity while optical properties were measured. The corresponding water adsorption−desorption isotherms and pore size distribution (PSD) are displayed in Figure 1A−C. Details for determining pore size distribution

(17) Boissiere, C.; Grosso, D.; Lepoutre, S.; Nicole, L.; Brunet Bruneau, A.; Sanchez, C. *Langmuir* **2005**, *21*, 12362.

using a modified Kelvin model are clearly given in a separate article.[17]

Film porosity characteristics are listed in Figure 1A−C. They clearly show that 2D hexagonal films are less porous with 15 vol % than 3D hexagonal and cubic ones with 43 and 54 vol %, respectively. This is consistent with the respective proportion of surfactant required to prepare each structure (CTAB:TEOS ratio = 0.10−0.18), except for the 2D hexagonal structure, which was expected to be more porous. This latter specific case is described further in this part. On one hand, $P6_3/mmc$ and $Pm3n$ structures display a quite similar behavior. Little adsorption takes place up to $P/P_0 = 0.41$ and 0.46, respectively, because of the filling of the micropores, which represent about 10% of the layer's volume. This is followed by a sudden steep increase that is associated with water capillary condensation inside the mesopores. Finally, the saturation of the porous network gives rise to the plateau at high relative pressure. Upon desorption, the similar, but inverse, phenomena occur. Desorption associated with mesopore emptying is, however, recorded at lower relative pressure than during adsorption, which results in the existence of hysteresis loops. These latter loops reflect the presence of pore interconnections or windows that are smaller than the average pore size, which is characteristic of bottle necks. Using a modified Kelvin's model,[17] we can deduce the average pore size and restriction from the given isotherms. In the present case, cubic and 3D hexagonal show 2.2 nm (1.3 nm restriction) and 1.9 nm (1.2 nm restriction) pore sizes, respectively. Pores sizes are of the same magnitude and their distribution is narrow, which is consistent with the same template being used for each preparation. In a first approximation, the slight variation of pore size suggests that the porosity has to be more accessible for the cubic structure than for the 3D hexagonal one. For both 3D structures, the system recovers its initial state when returning to a dry atmosphere, as evidenced by the adsorption and desorption branch superimposition below a partial pressure of 0.3. This latter observation is consistent with fully reversible systems that are stable to water uptake, as further confirmed by XRD after exposure to water (see Figures C and D in the Supporting Information). On the other hand, the $P6m$ structure has a disastrous response toward humidity. Indeed, the first isotherm of the film (see Figures E and F in the Supporting Information) is not interpretable, because adsorption is accompanied by a thickness reduction of 40%, which results in a great loss of porosity. As a result, the well-defined mesoporosity detected during adsorption is completely lost at the end of the first cycle. This network collapsing is attributed to capillary forces exerted during adsorption and reveals that 2D hexagonal films do not have sufficient rigidity to counterbalance such stresses, whereas 3D structures resist. The mesoporosity degradation has also been evidenced by XRD, as diagrams show the total disappearance of the (001) peak associated with the 2D hexagonal mesostructure after immersion of the film in water (see Figure B in the Supporting Information). It can eventually be concluded that hexagonally arranged cylinder pores around 2 nm in diameter and oriented parallel to the surface exhibit extremely weak resistance to water capillary stress. However, collapsed 2D hexagonal films exhibit a new isotherm (see Figure 1A) that keeps the characteristic shape of a microporous structure (15% vol porous) upon successive cycles, which confirms the irreversible transformation to micropores. Because no EEP model allows for the determination of micropore size distribution, we can state only that pores, resulting from the 2D structure collapsing, are less than 1 nm in diameter (which is the validity limit of the present Kelvin's model). In this study, for the sake of clarity, the water-collapsed 2D hexagonal structure will be labeled "2D-Hex-Col".

Mesoporous films prepared with F127 Pluronic block copolymer, used here for comparison purposes, are characterized by a cubic $Im3m$ mesophase (as checked by XRD, in agreement with previous studies[17]). Concerning the porous structure of these films, environmental ellipsometry analysis (see Figure G in the Supporting Information) brings three main results: (i) their porosity can be approximately divided into two contributions as 30 vol % mesoporosity and 10 vol % microporosity; (ii) the pore size distribution is narrow and corresponds to mesopores of 6.4 nm in diameter; (iii) the isotherm is fully reversible, indicating that the porous structure of the film is not affected at this stage. This last point is consistent with the results obtained for the 3D structured CTAB films. However, it has been shown previously that the contraction rate and the sensitivity to high humidity of the F127 templated films were higher than that of the CTAB-templated films.[17] This weaker global cohesion of the structure was ascribed to a lower (wall thickness)/(cell parameter) ratio and to a higher microporous volume.

Attending these EEP results, one expects the formal 2D hexagonal structure to be the less-accessible network, with porous cavities and restriction of less than 1 nm in diameter. Concerning 3D organized structures, one expects the cubic structure to be more accessible as a result of larger pores and higher porosity. One may argue on the restrictions that have the same dimension for both 3D structures, and we must take into account the relative number of these restrictions. Assessing such information is not straightforward by EEP, and we must here consider the structural difference to evaluate them. $Pm3n$ mesophase is defined by elongated micelles and $P6_3/mmc$ by spherical micelles.[7−18] Because elongated micelles are intermediate between channels and spheres, we suppose that a higher density of restriction is present in the 3D hexagonal structure (See Figure 1 schemes). In EEP, where condensation is governed by equilibrium between the vapor and liquid phases at a curved interface, these restrictions are the limiting factor for desorption but not for adsorption. This limitation completely hinders the vaporization of confined water above a critical relative pressure. On the other hand, when working with dissolved species in solution, the adsorption and migration of such species within the network are governed by other factors (concentration, steric hindrance, electrostatic interaction, film thickness, ...). The following part deals with electrochemical analyses of these films, providing information on mass-transfer processes through them.

(18) Aughlin, R. G. *The Aqueous Phase Behavior of Surfactants*; Harcourt Brace & Company: San Diego, 1996; p 216.

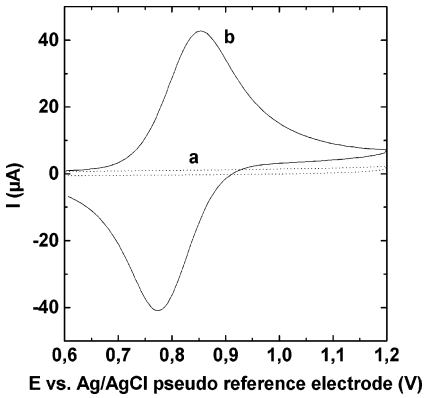

Figure 2. Cyclic voltammetric curves recorded in 0.05 M hydrogen phthalate solution (pH 4.1) containing 50 μM $Ru(bpy)_3^{2+}$ at ITO electrodes covered by mesoporous silica thin films with cubic symmetry (a) before and (b) after surfactant extraction with ethanol. The curves have been obtained from the same (geometric) electrode surface area at a scan rate of 100 mV s^{-1}. Potentials were measured versus a Ag/AgCl pseudo-reference electrode.

3.2. Electrochemical Characterization. Most experiments have been performed in 0.05 M hydrogen phthalate buffer (KHP) at pH 4.1 to prevent the dissolution of silica material and the associated destruction of the mesoporous architecture. This dissolution/destruction of the thin film could be important in more alkaline solution and/or in the presence of high concentration of salts, but it did not occurred in KHP solutions.[10] Several electroactive species displaying various charges and sizes ($Fe(CN)_6^{3-}$, $Ru(bpy)_3^{2+}$, I^-, and FcMeOH) have been used for characterizing the mass-transport processes into the thin mesoporous layers. The various materials have first been studied by cyclic voltammetry (CV) to get qualitative information of the influence of the mesostructure type on permeability into the thin film materials. In a second stage, some additional experiments have been performed with the wall-jet electrochemical technique in order to extract some quantitative data on permeability into the cubic phase mesoporous thin films. The various modified electrodes have been identified according to the mesostructure type of the films deposited onto the ITO surface: SiO_2-*Pm3n*-ITO (cubic phase), SiO_2-*P*6$_3$/*mmc*-ITO (hexagonal 3D), SiO_2-*P*6*m*-ITO (hexagonal 2D, which becomes in the presence of water 2D-Hex-Col), and SiO_2-*Im3m*-ITO (cubic phase obtained with F127 template).

3.2.1. Permeability Before and After Surfactant Extraction. Figure 2 depicts the CV responses recorded with SiO_2-*Pm3n*-ITO (a) before and (b) after surfactant extraction with ethanol (the effectiveness of template removal was checked by IR, see Figure H in the Supporting Information). The two experiments have been performed with the same electrode area in KHP solution containing 50 μM $Ru(bpy)_3^{2+}$.

Before extraction of the surfactant, no oxidation of the ruthenium species can be observed. The film seems to be totally closed to any external reagent. This demonstrates the high quality of the coating that appears to be crack-free with no noticeable defects. Any cracks would have resulted in measurable currents, as previously reported for "imperfect" sol−gel films on electrode surfaces.[19] The CV response observed in this case (see curve (a) on Figure 2) is typical of a purely capacitive behavior resulting from the charge and discharge of the electrode/solution interface. This also indicates that despite the barrier forbidding the transit of $Ru(bpy)_3^{2+}$ species, the film is not totally insulating for the external solution and electrical contact does exist at the electrode−solution interface (measured interfacial resistance of about 2 kΩ). Similar behavior has been observed with mesoporous titania thin films.[15]

After extraction of the surfactant a dramatic modification of the electrochemical response was observed and the CV curve was characterized by well-defined oxidation and reduction peaks, corresponding to the reversible $Ru^{II} \leftrightarrow Ru^{III}$ transformations (see curve (b) on Figure 2). Both oxidation and reduction peak currents were of high and equal intensities ($I_p^{ox} \approx I_p^{red} \approx 40$ μA), even higher than that on the bare ITO electrode (see below for explanation). The extraction of the surfactant obviously imparts an easy access of the redox probes to the ITO surface. All the film electrodes were thus studied after template extraction. In the next section, the electrochemical behavior of ITO electrodes modified with a cubic phase mesoporous thin film is compared to that observed at the bare ITO electrode and discussed as a function of the nature and concentration of redox probes.

3.2.2. Influence of the Nature and Concentration of the Electrochemical Probe. The nature of the redox probe, and especially its charge and size, has profound influence on the electrochemical response of the mesoporous silica films. This is illustrated in Figure 3 depicting the CV curves obtained on (a) bare ITO and (b) SiO_2-*Pm3n*-ITO modified electrodes in KHP solutions containing 500 μM I^- (Figure 3A), 500 μM $Fe(CN)_6^{3-}$ (Figure 3B), 50 μM FcMeOH (Figure 3C), and 50 μM $Ru(bpy)_3^{2+}$ (Figure 3D). The curves were obtained after a 15 min equilibration period (with forced convection) at a scan rate of 100 mV s^{-1} and using a pseudo-reference electrode (silver wire coated with AgCl). As shown, the voltammetric responses were extraordinarily different depending on the used probe. As the silica thin films are chemically and electrochemically inert under the experimental conditions applied here, the observed differences could be explained only by sieving effects and/or interactions between the mesoporous material and the redox probes. It should be reminded here that the silica surface, which has an IEP of about 2−3, thus bears negative charges at pH 4.1 (IEP = isoelectric point). This acidic IEP is mainly due to silanol−silanolate equilibria slightly shifted to the right (pKa value equal to 6.8 ± 0.2).[20] It is thus expected that these negative charges could have some influence on the permeation of electrochemical probes through the film via favorable or unfavorable electrostatic interactions.

The iodide/iodine redox couple is electrochemically irreversible on the ITO electrode, leading to strongly separated oxidation and reduction peaks at, respectively, 0.88 and −0.44 V versus the pseudo Ag/AgCl reference electrode (see curve (a) on Figure 3A). Oxidation of I^- on the bare ITO resulted in a peak current I_p^{ox} of 85 μA (at a scan rate of 100 mV s^{-1}). After modification with a cubic phase mesoporous thin film, the current intensity for I^- oxidation

(19) Sayen, S.; Walcarius, A. *Electrochem. Commun.* **2003**, *5*, 341.

(20) Schindler, P.; Kamber, H. R. *Helv. Chim. Acta* **1968**, *51*, 1781.

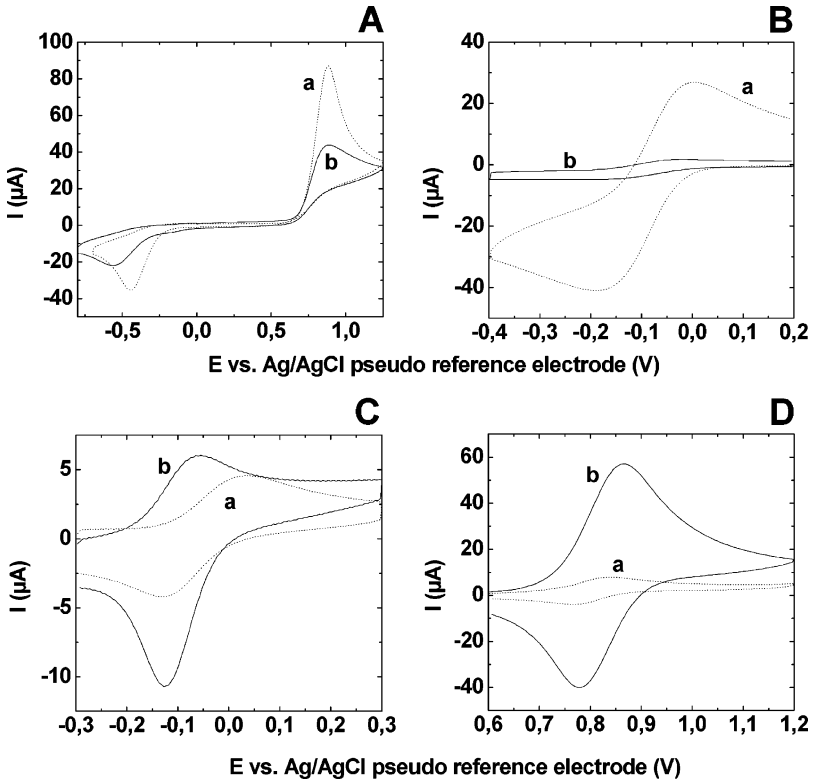

Figure 3. Cyclic voltammetric curves recorded in 0.05 M hydrogen phthalate solutions (pH 4.1) containing (A) 0.5 mM KI, (B) 0.5 mM $Fe(CN)_6^{3-}$, (C) 50 μM FcMeOH, and (D) 50 μM $Ru(bpy)_3^{2+}$ at a bare ITO electrode (dotted lines) and an ITO electrode covered by surfactant-extracted mesoporous silica thin films with cubic symmetry (plain lines). Other conditions are as in Figure 4.

decreased to 44 μA (see curve (b) on Figure 3A), whereas the peak potential did not change with respect to that on bare ITO, indicating that electron-transfer kinetics was not strongly affected by the presence of the mesoporous silica film. As a consequence, the difference in peak currents sampled at bare and modified ITO electrodes would essentially arise from mass-transfer limitations for I^- species into the mesoporous thin film. At this stage, it is not possible to distinguish unambiguously between steric hindrance and electrostatic repulsion to explain such restriction, but the latter effect is thought to be prominent because the size of the probe is much lower than the pore size (pore restriction of 1.3 nm).

The sieving effect was even more dramatic when using the bigger $Fe(CN)_6^{3-}$ probe holding more negative charges than I^-. Its electrochemical behavior on bare ITO is characterized by somewhat limited electron-transfer kinetics, leading to quite large peak potential separation, but displaying yet a rather well-defined peak shaped signal with a reduction peak current, $I_p^{red,}$ of about 40 μA (see curve (a) on Figure 3B). In the presence of the cubic mesoporous thin film, the electrochemical signal dropped now by more than 90% (see curve (b) on Figure 3B). This indicates a very restricted access to the ITO surface for the $Fe(CN)_6^{3-}$ species, as previously reported for this redox probe at other types of silica films coated onto electrode surfaces.[21] Enhancing the negative charge of the probe and increasing its size (passing from I^- to $Fe(CN)_6^{3-}$) thus resulted in hindering even more the access to the electrode surface. Again, the probe size (~0.7 nm) was much lower than that of the mesopores channels so that the electrostatic repulsions are expected to play a major role in the sieving behavior of the film. It is also interesting to mention a wave shaped contribution in the CV response (which might even be noticed on curve (b) on Figure 3B), suggesting a situation of partially blocked electrode surface displaying only small accessible areas separated from each other by a sufficient distance (the presence of pinholes acting as an ensemble of ultramicroelectrodes for which the electrochemical response is governed by radial diffusion[22]).

Using the neutral FcMeOH probe gave rise to a different behavior (Figure 3C). Contrary to the negatively charged species, the voltammetric peaks obtained for FcMeOH were on the same order of magnitude on both the bare ITO and SiO_2-*Pm3n*-ITO electrodes, the sampled currents being even slightly higher for the film-modified electrode (compare curves (a) and (b) on Figure 3C). It thus seems that the cubic mesoporous thin film does not hinder the probe diffusion to the electrode surface. Going into the details of the CV curves enables one to observe some differences between bare and thin-film-modified electrodes. First, the oxidation of FcMeOH occurs at lower potential with the modified ITO electrode ($E_p^{ox} = -0.06$ V) than on bare ITO ($E_p^{ox} = +0.03$ V), whereas reduction peaks appear at the same potential for both electrodes ($E_p^{red} \approx -0.12$ V). As a consequence, peak separations ($\Delta E = E_p^{ox} - E_p^{red}$) are 0.15 and 0.06 V, respectively, for the bare ITO and film-modified electrodes.

(21) (a) Deepa, P. N.; Kanungo, M.; Claycomb, G.; Sherwood, P. M. A.; Collinson, M. M. *Anal. Chem.* **2003**, *75*, 5399. (b) Collinson, M. M.; Moore, N.; Deepa, P. N.; Kanungo, M. *Langmuir* **2003**, *19*, 7669.

(22) Wightman, R. M.; Wipf, D. O. In *Electroanalytical Chemistry*; Bard, A. J., Ed.; Marcel Dekker: New York, 1989; Vol. 15, Chapter 3, pp 267−353.

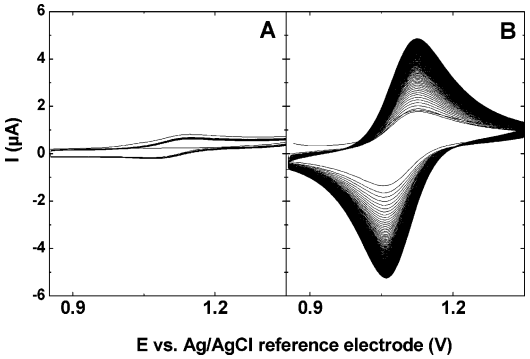

Figure 4. Multisweep cyclic voltammograms recorded in 0.05 M hydrogen phthalate solution (pH 4.1) containing 5 μM $Ru(bpy)_3^{2+}$ at (A) a bare ITO electrode and (B) an ITO electrode covered by a mesoporous silica thin film with cubic symmetry (surfactant extracted). CV measurements were performed immediately after immersion of the electrode in the (quiescent) solution, scan rate was 20 mV s^{-1}, and potentials were given versus a Ag/AgCl reference electrode.

The presence of the mesoporous silica film thus has a beneficial effect on the electrochemistry of FcMeOH, converting it from a quasi-reversible behavior on bare ITO to a reversible one on the film-modified electrode (the eventual contribution of adsorption of one form of ferrocene methanol is expected to be negligible, as peak currents were directly proportional to the square root of potential scan rate). Second, the reduction peak observed on scan reversal was twice as much on the modified electrode as on bare ITO. I_p^{red} was about 4 μA for the ITO electrode and more than 10 μA for the thin-film-modified ITO electrode. These differences can be explained by the positive charge held by the ferricinium ion $[FcMeOH]^+$ produced by oxidation of FcMeOH. This cation interacts favorably with the negatively charged silica matrix, which is likely to increase its effective concentration close to the electrode surface and facilitate the redox transformation of FcMeOH (by stabilizing the oxidation product).

Peak enhancement was even more impressive when performing the experiments with $Ru(bpy)_3^{2+}$ as the redox probe. As shown in Figure 3D major differences in peak currents were observed when passing from bare ITO to the SiO_2-*Pm3n*-ITO electrode, leading to CV peak intensities measured on the thin-film-modified electrode higher by about 1 order of magnitude with respect to those obtained on bare ITO (compare curves (a) and (b) on Figure 3D). This is clearly due to the accumulation of the positively charged $Ru(bpy)_3^{2+}$ and $Ru(bpy)_3^{3+}$ species into the mesostructured silica film because of favorable electrostatic interactions with the silica surface,[10,21b] leading to a significant increase in the local concentration of the electroactive species at the vicinity of the ITO electrode surface. It is noteworthy that CV curves were obtained after immersion of the electrodes under forced convection for ca. 15 min prior to measurement in the probe solution so that the accumulation was facilitated by this equilibration period.

Such preconcentration behavior is best evidenced by recording continuously multisweep CV measurements in rather diluted solutions. As an illustrative example, Figure 4 compares results obtained directly after the immersion of the SiO_2-*Pm3n*-ITO electrode (Figure 4B) in a solution containing 5 μM $Ru(bpy)_3^{2+}$ (150 successive CV scans at 20 mV s^{-1}) with the blank curves corresponding to the same experiment performed at bare ITO (Figure 4A). Upon scanning potentials continuously, a regular increase in peak currents was observed for both oxidation and reduction signals when using the film-modified electrode, whereas the same CV curve with signals of low intensity was always obtained on bare ITO. After 150 cycles, the CV peak currents recorded with the SiO_2-*Pm3n*-ITO electrode (4.6 μA) were more than 10 times higher than those on bare ITO (0.4 μA). Actually, it is difficult to estimate the concentration of $Ru(bpy)_3^{2+}$ species that have been accumulated in the film because one does not know its adsorption capacity. Anyway, this local concentration must be significantly higher than that in solution because peak currents measured by CV are directly proportional to the product $D^{1/2}C$ (D = diffusion coefficient and C = concentration of the probe); as diffusion into the film is expected to be slower than in solution, the probe concentration in the film must be much higher than that in solution to be consistent with the observed higher $D^{1/2}C$ product for the film-modified electrode. Accumulation into the mesoporous silica thin film occurred rather rapidly at the beginning of the experiment and then more slowly at low concentration of the probe in the solution because the quiescent conditions applied to get the CV curves enable mass transport only by diffusion. When performing similar experiment series in a more concentrated solution (i.e., 500 μM $Ru(bpy)_3^{2+}$), we reached the equilibrium more rapidly (after a few cycles) but the sensitivity gain was only 2-fold in comparison to the bare electrode, indicating a smaller contribution of the preconcentrated species to peak currents (relative to the solution-phase species). These data show that the CV response of the mesoporous silica film electrodes to cationic probes is the result of a complex combination of both diffusion of solution-phase species through the film to the electrode surface and accumulation of the molecular probe into the film. Depending on the probe concentration, one and/or the other parameter will govern the peak current intensity (mainly diffusion at high concentration and merely accumulation at trace levels). Anyway, both processes were diffusion-controlled as CV peak currents were always directly proportional to the square root of scan rate in agreement to the Randles−Sevcik equation.[16] This is notably illustrated in Figure I of the Supporting Information, via an example where accumulation is expected to be the major contribution of the voltammetric response (low concentration of the probe in solution).

At this stage, one can conclude that the mesoporous silica film acts as an electrostatic barrier for anions and as a preconcentration medium for cations with possible additional sieving effects due to the presence of a porous layer on the electrode surface. It is pointed out hereafter that the film structure was found to affect these processes to a great extent.

3.2.3. Comparison of p6m, $P6_3/mmc$, and Pm3n Porous Structures. The influence of the mesoporous silica thin film on its permeability to the redox probes was studied by cyclic voltammetry. Some illustrative results are depicted in Figure 5, where CV curves obtained at 50 mV s^{-1} in 0.5 mM (A) I^-, (B) $Fe(CN)_6^{3-}$, (C) FcMeOH, and (D) $Ru(bpy)_3^{2+}$ solutions using (a) SiO_2-*P6m*-ITO, (b) SiO_2-$P6_3/mmc$-ITO,

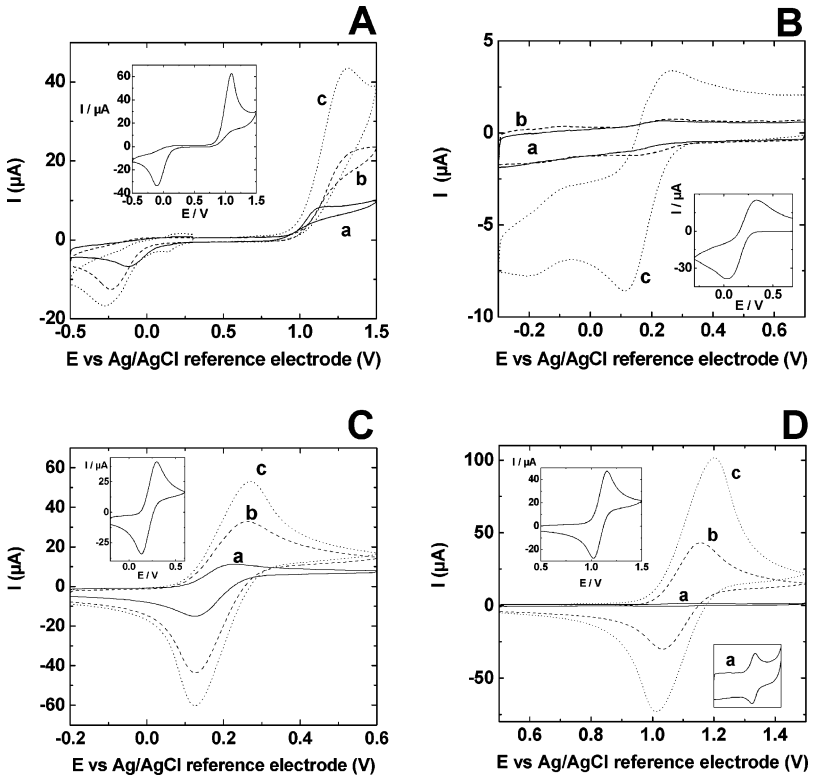

Figure 5. Cyclic voltammetric curves recorded in 0.05 M hydrogen phthalate solutions (pH 4.1) containing 0.5 mM (A) KI, (B) $Fe(CN)_6^{3-}$, (C) FcMeOH, and (D) $Ru(bpy)_3^{2+}$ at ITO electrodes covered by mesoporous silica thin films with (a) "2D-Hex-Col" symmetry, (b) 3D hexagonal symmetry, and (c) cubic symmetry. Scan rate was 50 mV s^{-1} and potentials were given versus a Ag/AgCl reference electrode.

and (c) SiO_2-*Pm3n*-ITO electrodes are reported. The electrochemical responses of the probes recorded on bare ITO in these conditions have been added as insets for comparison purposes. Note that this time, the CV curves have been obtained using a calibrated Ag/AgCl reference electrode so that all peak potentials are shifted by ca. 0.2 V in the positive direction in comparison to data presented in Figure 3. Analysis of the CV curves of Figure 5 reveals a very strong influence of the porous structure of the film on its permeability to the redox probes. The observed differences are also a dramatic function of the probe type. All the measurements have been repeated three times with three different electrodes modified with mesoporous silica films of the same porous structure.

Electrostatic Barrier and Resistance to Mass Transport. The CV signals for $Fe(CN)_6^{3-}$ (Figure 5B) were characterized by a quasi-absence of signal when using ITO covered by either 2D or 3D hexagonal mesostructures and a significant shielding effect for the cubic mesostructured film (with peak currents of very low values, i.e., 20% with respect to bare ITO). As discussed before, such a limitation is due to the electrostatic and/or sieving barrier that prevents the negatively charged redox probes from reaching easily the electrode surface. This time, however, significant difference was observed between the hexagonal and cubic structures, suggesting a possible effect of the internal organization of silica walls in the mesoporous film. Note that the very small signals observed with the 2D hexagonal thin film could be due to structural damage upon contacting water (see the discussion in section 3.1); however, this is not the unique reason, as peaks of very small intensities were also observed for the SiO_2-*P*6_3/*mmc*-ITO system, for which the silica mesostructure was kept mechanically stable in the presence of water (as demonstrated by XRD after exposure to high vapor pressure). It is also interesting to note that CV signals were always peak-shaped (with some wave contribution for SiO_2-*Pm3n*-ITO), confirming the homogeneous character of the films (the absence of millimeter-sized cracks). Distinction between the thin film structures was even better pointed out using the smaller I^- redox probe, bearing, however, a less yet negative charge. In this case, a clear hierarchy appeared in between the various mesostructures (Figure 5A): higher current values were measured with the cubic mesostructure (curve (c)), the signal then decreasing by about one-half with the 3D hexagonal mesostructure (curve (b)), and then again by a factor of 2 when passing to the 2D-Hex-Col mesostructure (curve (a)). Even if the electrostatic barrier induced by the negatively charged silica surfaces was operating in all the cases, the use of a smaller anionic probe bearing a smaller charge (I^- instead of $Fe(CN)_6^{3-}$) reveals that both size and electrostatic effects are likely to explain the lower voltammetric response of the mesostructured silica-film-covered ITO electrodes. The hierarchy $I_{cubic} > I_{3DHex} > I_{2DHex}$ was observed for the three electrodes. Resistance to mass transfer of I^- into the film was much lower than that for $Fe(CN)_6^{3-}$ species, as evidenced by current values recorded at the film-modified electrodes equal to 70, 35, and 15% of those sampled at bare ITO, respectively, for SiO_2-*Pm3n*-ITO, SiO_2-*P*6_3/*mmc*-ITO, and SiO_2-"*P*6*m*"-ITO electrodes.

Preconcentration Effects. The electrochemical detection of the large $Ru(bpy)_3^{2+}$ cation was also strongly affected by the porous structure of the film, showing again a sensitivity trend in the following sequence $I_{cubic} > I_{3DHex} > I_{2DHex}$ (Figure 5D). In this case, the response observed with the SiO_2-*Pm3n*-

ITO electrode was more than two times higher than that on bare ITO (compare curve (c) with the inset curve) because of the probe accumulation within the mesoporous silica film due to favorable electrostatic interaction (as discussed in section 3.2.2). Note that at such a high concentration (0.5 mM), $Ru(bpy)_3^{2+}$ accumulation was very fast, contrary to what happened in more diluted solutions (Figure 4). Accumulation was also much faster than that reported for the same cation at clay film electrodes, for which significantly slower processes have been reported[23] because of rather low apparent diffusion coefficients in the clay sheets (1×10^{-11} cm^2 s^{-1} range). This highlights the interest of the cubic mesostructure to impart high diffusion rates for guest species, which might be of great interest for electroanalytical purposes, as most electrochemical determinations at silica modified electrodes are diffusion-controlled.[8,24] The preconcentration behavior was also observed with the 3D hexagonal film, but the contribution of enhanced resistance to mass transport was found to hinder the advantage belonging to the accumulation; this leads to a significant (ca. 50%) decrease in peak currents for SiO_2-*P*6$_3$/*mmc*-ITO with respect to SiO_2-*Pm3n*-ITO (decrease of the apparent diffusion coefficient of $Ru(bpy)_3^{2+}$ in the film), yet they are on the same order of magnitude as those on bare ITO (compare curve (b) with the inset curve). Finally, the SiO_2-*P*6*m*-ITO electrode bearing the 2D-Hex-Col film gave rise to very low signals (see curve (a) on Figure 5D), yet well-defined and peak-shaped, with intensities of about 2% relative to those obtained on bare ITO. This demonstrates unambiguously the restricted mass-transfer rates in the 2D-Hex-Col thin film, as $Ru(bpy)_3^{2+}$ species are not expected to be excluded from the material on the basis of their charge, but the ingress of such large cations (1.1 nm in average diameter[25]) in the less-open film are likely to undergo long-distance order alteration and mesopore collapse in aqueous medium (pore diameter <1 nm).

It is also interesting to note that detection of I^- (sizing 0.36 nm in its hydrated form[26]) at the SiO_2-*P*6*m*-ITO electrode, in spite of its negative charge, was 10 times more sensitive than the $Ru(bpy)_3^{2+}$ response, confirming once again the possible role played by the probe size in addition to charge selectivity. By an appropriate choice of the film porous topology, it is thus possible to tune the recognition properties of the mesoporous silica layer from charge to size selectivity. For example, the SiO_2-*Pm3n*-ITO electrode enabled the sensitive detection of $Ru(bpy)_3^{2+}$ species while rejecting the $Fe(CN)_6^{3-}$ ones (charge selectivity), whereas satisfactory detection of I^- and poor sensitivity to $Ru(bpy)_3^{2+}$ were achieved with the SiO_2-*P*6*m*-ITO electrode (size selectivity arising from diffusional limitations). The SiO_2-*P*6$_3$/*mmc*-ITO electrode behaved intermediately by displaying CV responses monitored by both electrostatic repulsion or preconcentration and sieving effects.

Table 1. Normalized Peak Currents Sampled by Cyclic Voltammetry for the Various Mesoporous Silica Film Electrodes Relative to the Bare ITO Electrode (conditions as in Figure 5; pore sizes (diameters and restrictions) of the materials are also included)

	SiO_2-*P*6$_3$/*mmc*	SiO_2-*Pm3n*	SiO_2-*P6m*	SiO_2-*Im3m*
pore diameter (nm)	1.9	2.2	<1	6.4
restriction (nm)	1.2	1.3	<1	3.4
I_{film}/I_{ITO}				
$Fe(CN)_6^{3-}$ (0.7 nm)	~0	0.2	~0	0.04
I^- (0.25−0.36 nm)	0.4	0.7	0.1	0.4
$Ru(bpy)_3^{2+}$ (1.1 nm)	0.9	2.1	~0	0.3
$FcCH_2OH$ (0.45 nm)	0.8	1.3	0.3	0.4

Some illustrative results of CV experiments performed in the presence of FcMeOH are given in Figure 5C. They also indicate a significant influence of the mesoporous structure on the peak height, leading to the same sensitivity scale as for $Ru(bpy)_3^{2+}$: $I_{cubic} > I_{ITO} > I_{3DHex} > I_{2DHex}$. In this case, however, the differences between the various electrodes were less pronounced. On the one hand, the preconcentration effect on SiO_2-*Pm3n*-ITO was less, because only the oxidation product, $[FcMeOH]^+$, was positively charged (the starting analyte, FcMeOH, was neutral and not expected to be involved in electrostatic interactions). On the other hand, the CV response observed with using the SiO_2-*P*6*m*-ITO electrode was less affected by the sieving effect of the 2D-Hex-Col film, which is explained by the smaller size of FcMeOH (0.45 nm) relative to $Ru(bpy)_3^{2+}$ (1.1 nm).[25] Another difference is related to the anodic-to-cathodic currents ratio that was slightly superior to unity for ruthenium species (this was probably due to different affinities between $Ru(bpy)_3^{2+}$ and $Ru(bpy)_3^{3+}$ for the silica surface in this pH conditions), whereas the reduction peak currents were systematically higher than the oxidation ones for FcMeOH (due to possible preconcentration of the electrogenerated $[FcMeOH]^+$ species into the film, as discussed above).

A summary of the above data is given in Table 1, in the form of the "normalized" peak currents (obtained for the various films relative to the bare electrode) for each redox probe considered here, confirming the trends discussed above. Table 1 also contains data relative to the mesoporous film prepared from the F127 Pluronic template (cubic material with larger pores). Unexpectedly, on the basis of the larger pore size of this film (in comparison to the CTAB-based structure), we found that peak currents measured with SiO_2-*Im3m*-ITO were significantly lower than those measured with SiO_2-*Pm3n*-ITO, indicating stronger resistance to mass transport to the electrode surface and lower preconcentration efficiency. This latter point can be explained by the lower amount of silanol groups in materials obtained by calcination relative to those for which template was removed by solvent extraction. The restricted permeability is much more unexpected, as mass-transport rates in mesoporous materials usually increased as pore size was larger.[27] A possible explanation could be the degradation of the mesostructure in the presence of water, which is sustained by significant porosity loss of this material after repetitive use

(23) Ghosh, P. K.; Bard, A. J. *J. Am. Chem. Soc.* **1983**, *105*, 5691.
(24) (a) Audebert, P.; Walcarius, A. In *Functional Hybrid Materials*; Gomez-Romero, P., Sanchez, C., Eds.; Wiley-VCH: Weinheim, Germany, 2004; Chapter 6, pp 172−209. (b) Walcarius, A. In *Encyclopedia of Nanoscience and Nanotechnology*; Nalwa, H. S., Ed.; American Scientific Publishers: Stevenson Ranch, CA, 2004; Vol. 2, pp 857−893. (c) Walcarius, A. *Chem. Mater.* **2001**, *13*, 3351. (d) Walcarius, A. *Electroanalysis* **2001**, *13*, 701.
(25) Bélanger, S.; Hupp, J. T.; Stern, C. L.; Slone, R. V.; Watson, D. F.; Carrell, T. G. *J. Am. Chem. Soc.* **1999**, *121*, 557.
(26) Marcus, Y. *Ion Solvation*; Wiley: Chichester, U.K., 1985.
(27) Walcarius, A.; Etienne, M.; Lebeau, B. *Chem. Mater.* **2003**, *15*, 2161.

in solution (see Figure G in the Supporting Information). These data point out the important role of the film preparation mode on its performance when used in aqueous medium, showing an advantage for CTAB-based 3D films over the F127-based one, in agreement with the lower contraction rates observed for CTAB films in the presence of water.[17]

The effect of pH was also studied to further support the charge selectivity behavior. Some illustrative results are depicted in Figure J of the Supporting Information for the SiO_2-*Im3m*-ITO electrode and two redox probes of different charge (I^- and $Ru(NH_3)_6^{3+}$). When passing from pH 4 (where the silica surface is negatively charged) to pH 1 (i.e., below the IEP of silica, where positive charges are present of its surface), the electrochemical response of SiO_2-*Im3m*-ITO to the positively charged redox probe was found to drop dramatically because of unfavorable electrostatic interactions, whereas the response to the negatively charged one was found to grow as a result of preconcentration of the probe. Though not so selective as organically modified silicate films bearing organo-functional groups with net positive or negative charges,[28] these data suggest a possible tuning of ion-exchange properties of mesoporous silica films by appropriate pH change.

The above results demonstrate that the way of preparing mesoporous silica thin films on a solid electrode surface, and especially their structure, has a great influence on their permeability to solution-phase redox probes. For the mesostructure types studied here, the resistance to mass transport was observed to increase when passing from the cubic structure to the 3D hexagonal one, with the 2D hexagonal system being even more restricting (probably due to some degradation of the mesoporous architecture in the presence of water, which was also true to a lesser extent for the cubic film with larger pores prepared from the block copolymer). As expected, these effects were more constraining for redox probes of bigger sizes and films of smaller pore sizes. Moreover, because of the negative charge bearing by the silica surface, these films acted as a permselective barrier likely to exclude anions (at least partially, depending on their size and density of negative charges) and to preconcentrate cations more effectively as their concentration in solution was lowered. Opposite behavior was observed when working at pH values below IEP. The whole electrochemical behavior is directly related to these mass-transfer processes and thus results from a complex combination of sieving effects and permselective properties, which are dramatically dependent on the porous structure of the film, the guest properties (charge, size), and the solution-phase concentrations. As no measurable overpotentials were observed when passing from bare ITO to the modified electrodes, it is likely that the mesoporous thin films did not affect the electron-transfer kinetics at the ITO−silica film interface.

3.2.4. Influence of the Film Thickness (P6₃/mmc Mesostructure). Sieving and preconcentration effects are also expected to be influenced by the film thickness. This has been investigated using ITO electrodes covered with meso-

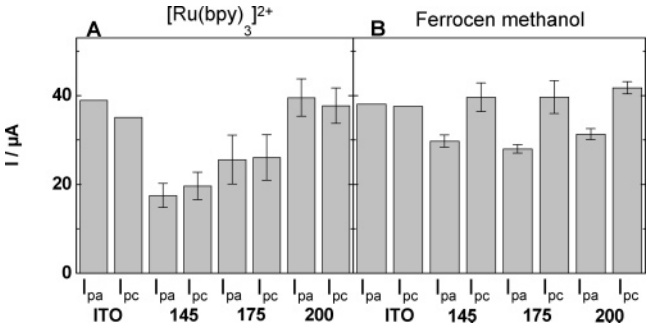

Figure 6. Comparison of average peak currents (both anodic, I_{pa}, and cathodic, I_{pc}) measured by cyclic voltammetry (50 mV s^{-1}) in 0.05 M hydrogen phthalate solution (pH 4.1) containing 0.5 mM (A) $Ru(bpy)_3^{2+}$ or (B) FcMeOH on a bare ITO electrode (ITO), and ITO electrodes covered by mesoporous silica thin films with 3D hexagonal symmetry displaying different thicknesses: 145, 175, and 200 nm. For each family of films, peak currents have been measured from experiments performed with three different electrodes prepared in the same conditions; reported data are the average values (with their corresponding standard errors).

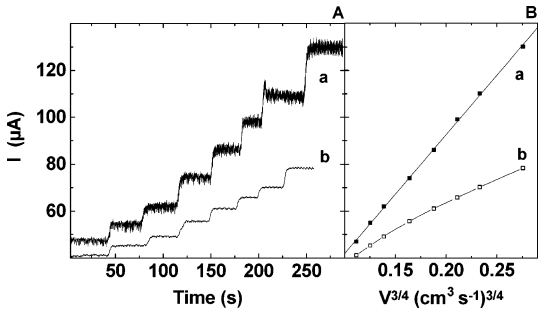

Figure 7. (A) Typical chronoamperograms obtained by wall-jet electrochemistry on (a) bare ITO and (b) SiO_2-*Pm3n*-ITO electrodes in a solution containing 1 mM $Ru(bpy)_3^{2+}$. The solution flow rate was varied here from 0.054 to 0.179 cm^3 s^{-1}. The applied potential was +1.2 V versus a Ag/AgCl pseudo-reference electrode. (B) *I* versus $V^{-3/4}$ plot of the corresponding chronoamperograms.

porous silica films displaying 3D hexagonal mesostructures (chosen here because they are more restrictive than the cubic ones and more mechanically stable than the 2D-Hex-Col ones) and characterized by thicknesses of 145, 175, and 200 nm. CV experiments have been performed in solutions containing either $Ru(bpy)_3^{2+}$ or FcMeOH as the redox probes, both at a concentration of 5×10^{-4} M. Mean values of peak currents (from triplicate) have been reported in parts A ($Ru(bpy)_3^{2+}$) and B (FcMeOH) of Figure 6. Despite the significant variability inherent in such a characterization of different film electrodes, a real tendency can be extracted from the averaged peak intensity values. For $Ru(bpy)_3^{2+}$ species that are likely to accumulate in the film because of their positive charge but also to undergo transport restriction in porous medium because of their large size, peak currents sampled at the SiO_2-$P6_3/mmc$-ITO electrode were on the same order of magnitude (200 nm thick film) or lower (145 and 175 nm thick films) than at bare ITO. Such lower sensitivity can be attributed to lower mass-transfer rates induced by the presence of the mesoporous film on the electrode surface. Interestingly, peak intensities were found to be proportional to the film thickness, with thicker films leading to higher peak currents, indicating that the thicker the film, the higher the amount of accumulated ruthenium species. It thus seems that preconcentration into the film is more effective when the film thickness is increased. Performing similar experiments with FcMeOH as the redox

(28) (a) Hsueh, C.; Collinson, M. M. *J. Electroanal. Chem.* **1997**, *420*, 243. (b) Wei, H.; Collinson, M. M. *Anal. Chim. Acta* **1999**, *397*, 113.

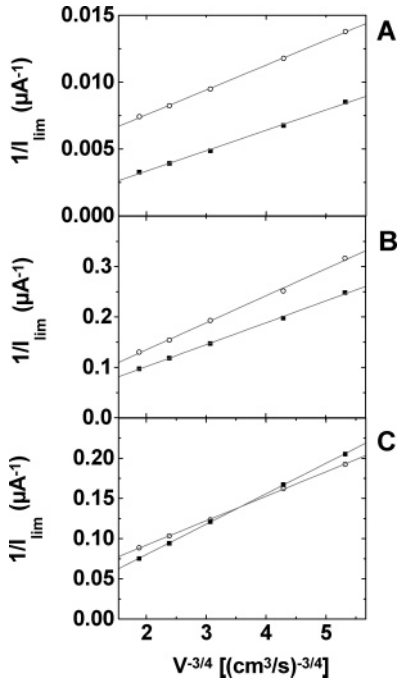

Figure 8. $1/I_{lim}$ versus $V^{-3/4}$ plots obtained from chronoamperometry experiments performed in 0.05 M hydrogen phthalate solutions containing (A) 500 μM KI, (B) 50 μM FcMeOH, or (C) 50 μM $Ru(bpy)_3^{2+}$, using a bare ITO electrode (solid square) and an ITO electrode modified with a mesoporous silica thin film with cubic symmetry (open circle).

probe resulted in a different behavior. This time, the observed currents remain rather independent of the film thickness. This can be explained by the fact that the presence of such a 3D hexagonal mesoporous film on the electrode does not significantly hinder the diffusion of the rather small FcMeOH probe to the electrode surface. Again and as already discussed above, reduction peaks were characterized by higher current intensities and noteworthy higher variability than the corresponding oxidation signals.

3.2.5. Wall-Jet Electrochemical Experiments. Using electroactive probes enables to quantify molecular transport through thin films by electrochemical methods such as on wall-jet electrochemistry[29] or rotating disk voltammetry.[30] Here, we have applied the method developed and validated by Massari et al.[31] on the basis of wall-jet electrochemistry to determine the permeabilities (i.e., product of diffusion coefficient in the film, D_f, and solution-to-film partition coefficient, P) of redox species into the cubic mesoporous thin films. The CTAB-based cubic structure has been selected because it appears to be the most promising film for practical applications (i.e., electrochemical sensing) because of its open structure likely to induce high sensitivity to the modified electrode, and the F127-based one for comparison purposes.

The experimental setup (see the scheme in Figure K of the Supporting Information) consists of a specially designed wall-jet cell at the bottom of which was placed the studied electrode, its working surface area defined by an O-ring. A syringe capillary was positioned perpendicularly to the electrode surface at a distance of 1 mm and the solution was flowed through it in the direction of the electrode surface at selected volume flow rates, V, as monitored by a peristaltic pump. Applying a constant V of solution allowed us to measure a steady-state current (i.e., diffusion-limited current, I_{lim}); increasing this flow rate resulted in a corresponding increase of I_{lim}. This is illustrated in Figure 7A, which depicts two chronoamperograms measured on bare ITO (curve a) and SiO_2-*Pm3n*-ITO (curve b) electrodes using $Ru(bpy)_3^{2+}$ as the redox probe. As expected, strengthening the convection conditions (increasing V) led systematically to an increase in the measured limiting currents, which was linear for ITO but tended to a plateau for the SiO_2-*Pm3n*-ITO electrode when expressed as a function of $V^{3/4}$ (Figure 7B). The analytical expression describing the relationship between the applied volume flow rate, V, and the diffusion-limited current, I_{lim}, for a porous thin film coated on a solid electrode surface is given by eq 1[31]

$$\frac{1}{I_{lim}} = \frac{1}{I_{MT}} + \frac{1}{I_{perm}} = \frac{\nu^{5/12}\alpha^{1/2}}{1.38nFCD_S^{2/3}V^{3/4}R^{3/4}} + \frac{d}{nFA(PD_f)C} \quad (1)$$

where d is the thickness of the thin film membrane, n the number of exchanged electrons, F the Faraday constant, A the surface area of the electrode (defined by the O-ring), and α the diameter of the solution jet; P and D_f have been defined above, and C is the concentration of electroactive species in the solution. The first term of the equation ($1/I_{MT}$) is related to solution-phase mass transport (I_{MT} is the current due to mass transport through solution) and the second term ($1/I_{perm}$) to permeation through the film. By increasing the V of solution, the first term of the equation ($1/I_{MT}$) tends to zero, and the relationship simplifies to become eq 2

$$\frac{1}{I_{lim}} = \frac{1}{I_{perm}} = \frac{d}{nFA(PD_f)C} \quad (2)$$

Therefore, plotting $1/I_{lim}$ versus $V^{-3/4}$ enables one to determine the permeation current and thus the permeability of the molecular probes into the mesoporous thin film via the y intercept of the curve.

Typical $1/I_{lim}$ versus $1/V^{3/4}$ plots have been reported in Figure 8, corresponding to experiments performed with bare ITO (line a) and SiO_2-*Pm3n*-ITO (line b) electrodes in the presence of 0.5 mM I^- (Figure 8A), 0.05 mM FcMeOH (Figure 8B), and 0.05 mM $Ru(bpy)_3^{2+}$ (Figure 8C). For all the experiments (on both bare ITO and SiO_2-*Pm3n*-ITO electrodes), a linear relationship was observed between $1/I_{lim}$ and $1/V^{3/4}$ with correlation coefficients higher than 0.999. It

(29) Yamada, J.; Matsuda, H. *J. Electroanal. Chem.* **1973**, *44*, 189−198.
(30) (a) Gueshi, T.; Tokuda, K.; Matsuda, H. *J. Electroanal. Chem.* **1979**, *101*, 29. (b) Peerce, P. J.; Bard, A. J. *J. Electroanal. Chem.* **1980**, *114*, 89. (c) Stevens, N. P. C.; Rooney, M. B.; Bond, A. M.; Feldberg, S. W. *J. Phys. Chem. A* **2001**, *105*, 9085. (d) Leddy, J.; Bard, A. J. *J. Electroanal. Chem.* **1983**, *153*, 223. (e) Saveant, J. M. *J. Electroanal. Chem.* **1991**, *302*, 91. (f) Ikeda, T.; Schmehl, R.; Denisevich, P.; Willman, K.; Murray, R. M. *J. Am. Chem. Soc.* **1982**, *104*, 2683. (g) Gough, D. A.; Leypoldt, J. K. *Anal. Chem.* **1979**, *51*, 439. (h) Ewing, A. G.; Feldman, B. J.; Murray, R. W. *J. Phys. Chem.* **1985**, *89*, 1263.
(31) Massari, A. M.; Gurney, R. W.; Schwartz, C. P.; Nguyen, S. T.; Hupp, J. T. *Langmuir* **2004**, *20*, 4422.

Table 2. Permeation Characteristics of the SiO_2-*Pm3n* Film Measured with I^-, FcMeOH, and $Ru(bpy)_3^{2+}$ Electroactive Molecular Probes

molecular probe (diameter)	$10^6 \times$ Ds ($cm^2\ s^{-1}$)	Cs (mM)	I_{lim} (mA)	$10^3 \times PD_f/d$ ($cm\ s^{-1}$)	$10^7 \times PD_f$[a] ($cm^2\ s^{-1}$)
I^- (2.5 Å; 3.6 Å if hydrated)	19.9[31]	0.5	262	10.9	1.6
FcMeOH (4.5 Å)	7.8[31]	0.05	79	32.7	4.9
$Ru(bpy)_3^{2+}$ (~11 Å)	2.6[10]	0.05	3.3	1.4	0.2

[a] Estimated for $d = 150$ nm.

Table 3. Permeation Characteristics of the SiO_2-*Im3m* Film Measured with I^-, FcMeOH, and $Ru(bpy)_3^{2+}$ Electroactive Molecular Probes

molecular probe (diameter)	$10^6 \times$ Ds ($cm^2\ s^{-1}$)	Cs (mM)	I_{lim} (mA)	$10^3 \times PD_f/d$ ($cm\ s^{-1}$)	$10^7 \times PD_f$[a] ($cm^2\ s^{-1}$)
I^- (2.5 Å; 3.6 Å if hydrated)	19.9[31]	0.5	49	2.09	0.32
FcMeOH (4.5 Å)	7.8[31]	0.5	18	0.75	0.12
$Ru(bpy)_3^{2+}$ (~11 Å)	2.6[10]	0.5	4.5	0.19	0.03

[a] Estimated for $d = 150$ nm.

is noteworthy that the slopes of these curves would have been parallel to each other according to eq 1, which was not exactly the case especially for $Ru(bpy)_3^{2+}$ species. Nevertheless, it was possible to evaluate the permeability data (related to the plateau current at very high flow rate), which were extracted from the *y* intercept of these curves, by considering the film thickness (150 nm), electrode surface area (0.50 cm^2) and concentration of the probe in solution; these data have been gathered in Table 2. The PD_f product is typically reported as a measure of molecular transport.[31]

It clearly appears that permeability is strongly dependent on both size and charge of the molecular probe. The hierarchy observed using wall-jet electrochemistry is FcMeOH (4.9×10^{-7} $cm^2\ s^{-1}$) > I^- (1.6×10^{-7} $cm^2\ s^{-1}$) > $Ru(bpy)_3^{2+}$ (0.2×10^{-7} $cm^2\ s^{-1}$). One can reasonably assume a value for solution-to-film partition coefficients close to unity for I^- and FcMeOH species, as these probes are not likely to accumulate within the mesoporous silica thin film. One can therefore consider the PD_f values as being very close to the apparent diffusion coefficients of I^- and FcMeOH in the thin film displaying a cubic mesostructure. These results demonstrate the great permeability of the film, as the diffusion coefficient for FcMeOH was only 16 times lower than that in solution, whereas transport rates for I^- in the film dropped by 2 orders of magnitude with respect to diffusion in solution (Table 2). Once again, the permeability values measured with the F127-based cubic film (SiO_2-*Im3m*-ITO) were found to be lower (by about 1 order of magnitude, see Table 3) than those obtained for SiO_2-*Pm3n*-ITO. On the basis of steric considerations, it could be rather surprising that the smaller probe I^- (3.6 Å when hydated[26]) appeared to permeate at slower rates than FcMeOH (4.5 Å). This behavior is due to the aforementioned negatively charged silica surface acting as an electrostatic barrier, somewhat hindering permeation of the negatively charged probes. A similar experiment has been performed with $Fe(CN)_6^{3-}$; however, the limiting current I_{lim} did not reach steady-state values, and no permeation information can thus be extracted from it, indicating the quasi absence of permeability for species as negatively charged and as big as $Fe(CN)_6^{3-}$. Note that such electrostatic-based constraints have been previously reported to slow down mass-transfer processes in mesoporous silica particles even though diffusion in such ordered mesostructures is usually fast in comparison to molecular transport in the corresponding non-ordered silica gels.[32] This was notably the case when attempting to protonate amine-functionalized mesoporous silica materials, for which reaction rates were found to fall dramatically as the extent of protonation increased due to increasingly restricted ingress of protons in the mesoporous solid containing an increasing amount of positive charges (ammonium groups) on the mesopore walls.[27]

The case of $Ru(bpy)_3^{2+}$ has to be treated differently, as this cation can be accumulated to a significant extent in the mesoporous silica film as a consequence of favorable electrostatic interactions with the silica surface. Considering first the PD_f product in the discussion shows that molecular transport of the large $Ru(bpy)_3^{2+}$ species into the film is 25 times lower than that of the smaller FcMeOH probe (Table 2). But partition coefficients, *P*, of $Ru(bpy)_3^{2+}$ into the film are expected to be higher than unity and to vary as a function of its concentration in solution. Even it was not so easy to evaluate these values, we have tried to determine approximately the concentration of $Ru(bpy)_3^{2+}$ into the film in the same experimental conditions as those applied in the electrochemical experiments. This led to a value of *P* estimated as about 50, which is much higher than those values reported previously for a thin mesoporous silica film displaying 2D-Hex nanostructure (3.2 and 1.6).[10] On the basis of this *P* value and comparing *Pm3n* and *P6m* films, it appeared that diffusion of $Ru(bpy)_3^{2+}$ is much faster into the cubic mesoporous film (D_f equal to about 4×10^{-10} $cm^2\ s^{-1}$) than in 2D hexagonal mesoporous film[10] (D_f in the 1×10^{-12} $cm^2\ s^{-1}$ range). The same experiments have been performed with the F127-based cubic film (SiO_2-*Im3m*-ITO, see Table 3), giving rise to a lower permeability than for SiO_2-*Pm3n*-ITO (Table 2) and confirming again the above cyclic voltammetry results (Table 1), which is thought to be mostly due to the lower structural integrity of the F127-based material in aqueous medium, as discussed above.

4. Conclusions

This study demonstrates that the nanoporous structures (*P6m*, $P6_3/mmc$ or *Pm3n*) of mesoporous silica thin films prepared on a solid electrode surface has a great influence on their permeability to solution-phase redox probes. Mass transport rates were found to decrease when passing from

(32) (a) Walcarius, A.; Etienne, M.; Bessiere, J. *Chem. Mater.* **2002**, *14*, 2757. (b) Walcarius, A.; Delacôte, C. *Chem. Mater.* **2003**, *15*, 4181.

the cubic structure to the 3D hexagonal one and then to the "collapsed 2D hexagonal" system, which was the most restricting one, probably because of some degradation of the mesoporous architecture in the presence of water. The electrochemical signals were found to be lower for the redox probes of bigger sizes, and their intensity was greatly affected by either permselective or preconcentration behaviors. Indeed, the negatively charged silica surface acted as a permselective barrier likely to exclude anions (partially or totally, depending on their size and density of negative charges) or as an accumulation medium likely to concentrate cations more effectively as their concentration was lowered in the solution. finally, wall-jet electrochemistry studies have allowed to extract permeability values for the following redox probes in the cubic mesoporous film of *Pm*3*n* structure: FcMeOH (4.9×10^{-7} cm^2 s^{-1}) > I^- (1.6×10^{-7} cm^2 s^{-1}) > $Ru(bpy)_3^{2+}$ (0.2×10^{-7} cm^2 s^{-1}), the hierarchy of which was governed by the size and charge of the probes. In spite of its larger pore size, the F127 block copolymer-based film gave rise to less efficient reduction/oxidation processes than the CTAB-based ones, highlighting the importance of both the preparation of the materials (i.e., nature of the template) and the stability of the film (structural integrity) in aqueous medium.

Acknowledgment. This work has been performed under the umbrella of a CNRS GdR entitled "Matériaux Hybrides Organisés Multifonctionnels" (MHOM, GDR 2922).

Supporting Information Available: TEM images, SAXS diagrams, X-ray diffractograms, various adsorption−desorption graphs, CV curves, and schematic of the wall-jet setup. This material is available free of charge via the Internet at http://pubs.acs.org.

CM0625068